scientific reports

Check for updates

OPEN

Lossless single-molecule counting to absolute quantify proteoforms

Tobias Gross[1,2], Tobias Hundertmark[1,2], Villő Csiszár[4], András Attila Sulyok[3], Nina Gross[2], Maike Breiden[6], Niklas Kitschen[6], Uritza von Groll[6], Christoph Niemöller[2], Pablo Sánchez-Martín[2], Anne Heine[7], Jens Göpfert[7], Tamás Szórádi[2], Philipp Lübbert[2], Peter Koltay[1,2], Peter Porschewski[6], Roland Zengerle[5] & Csaba Jeney[2]✉

A novel immunoassay, termed Protein Interaction Coupling (PICO), is introduced to deliver clear, reference-free quantification of proteoforms - precise quantification. PICO employs a compartmentalized, homogeneous single-molecule assay with lossless and sensitive signal generation, capable of detecting down to a few molecules per reaction. Additionally, it utilizes a background-free, digital enumeration principle, known as decouplexing. PICO is presented as mathematical theories, providing a theoretical understanding of its chemistry. Consequently, PICO demonstrates precise quantification, as exemplified with recombinant and non-recombinant ErbB2 and multi-tagged peptide rTRX targets, validating quantification against internal and external references in both analytical and cellular matrices. Furthermore, PICO enables combinatorial multiplexing (cplex), a readout between any two antibodies, demonstrated by an 8-plex antibody, 12-cplex PICO, measuring functional changes of the ErbB pathway upon mock and dactolisib treatment delivering quantitative cellular stoichiometry. PICO possesses significant potential for versatile, standardized, and accurate protein measurements, offering insights into physiological and perturbed cellular processes.

The labyrinthine complexity of the human genome is a marvel to behold. The expressed proteome is a realm of staggering complexity, boasting an estimated one million proteoforms[1]. A particularly salient chemical attribute is the dynamic concentration of proteoforms including proteins, PPIs (protein interaction), PTMs (post-translational modification) and overall material (and information) flows through the networks, as these serve as the primary regulated chemical actors related to the physiology of living cell. Monitoring the proteoforms has been a major aim of protein analytical methods[2], however, a significant challenge that persists is the accurate determination of absolute protein concentrations with universal comparability between measurements especially between different proteoforms.

Generally, absolute quantitative protein assays[3] based on no reference require a readout method ensuring there is no off-setting background signal, i.e. having zero background, and that the generated quantitative signal is robust, capable of providing lossless molecular counts in a wide and linear dynamic range, i.e. absolute signal. These are seemingly conflicting requirements due to the required extreme signal-to-noise performance. Due to these hurdles, absolute quantificative analytical methods are only partially established in the study of biological systems, and mainly based on mass spectrometry techniques[4]. Methods without using external quantitative standards, avoiding unreliabilities sourced form the vastly different qualities of quantitative protein standards, are especially scarce. Specifically for immunoassays a reference-free absolute quantification is not yet established despite the significant advance in digital immunoassays, exemplifying the most advanced technologies including SIMOA and others[5,6].

Building on these state-of-the-art technologies (Table C1), recent innovations in digital immunoassays have transformed protein quantification, addressing the critical challenge of detecting low-abundance proteoforms with remarkable precision and sensitivity. Digital immunoassays such as Single Molecule Arrays (Simoa) have led the way by enabling close single-molecule sensitivity, facilitating early diagnostics, and allowing analysis of trace proteins at the attomolar level-a sensitivity that conventional methods such as ELISA could not achieve[7]. However, for applications requiring even more refined sensitivity or multiplexed analysis, traditional Simoa still

[1]Laboratory for MEMS Applications, Department of Microsystems Engineering, University of Freiburg, Georges-Köhler-Allee 103, Freiburg 79110, Germany. [2]Actome GmbH, Georges-Köhler-Allee 302, Freiburg 79110, Germany. [3]Faculty of Information Technology and Bionics, Pázmány Péter Catholic University, Práter Street 50/A, Budapest, Hungary. [4]Department of Probability Theory and Statistics, Institute of Mathematics, Eötvös Loránd University, Pázmány Péter sétány 1/C, Budapest 1117, Hungary. [5]Hahn-Schickard, Georges-Köhler-Allee 103, Freiburg 79110, Germany. [6]QIAGEN, Qiagen Strasse 1, Hilden 40724, Germany. [7]NMI Natural and Medical Sciences Institute at the University of Tübingen, Markwiesenstraße 55, Reutlingen, Germany. ✉email: csaba.jeney@actome.de

presents limitations, particularly in sample throughput and adaptability to point-of-care settings[6]. Advanced methodologies like dropcast single molecule assays (dSimoa) and Molecular On-bead Signal Amplification for Individual Counting (MOSAIC) have pushed digital immunoassays further. These techniques improve both sensitivity and sampling efficiency, a critical factor for detecting extremely low concentrations of biomarkers [6]. The MOSAIC platform, for example, achieves high-throughput digital detection by integrating flow cytometric readouts, which enhances multiplexing capabilities and makes it feasible to detect a variety of biomarkers simultaneously, even in resource-limited settings[8]. Additionally, the use of one-pot, wash-free digital immunoassays like those developed by Byrnes et al. greatly reduces complexity, making them ideal for more accessible, streamlined diagnostic applications[9]. Complementing these advances, proximity-based assays have introduced new avenues for highly multiplexed protein detection. Proximity ligation assays (PLA) and proximity extension assays (PEA), for instance, are enabling highly sensitive, simultaneous detection of multiple protein interactions and modifications, crucial for studies that require multiplexed data in a single assay[10]. PLA uses a unique approach involving triple-binder strategies that allows detection of individual protein molecules at extremely low abundance, thereby widening the range of detectable proteins and enhancing specificity by requiring three recognition events for signal generation[11]. PEA, on the other hand, couples with next-generation sequencing (NGS) to facilitate ultra-high-throughput proteomics with minimal sample input, offering a powerful tool for precision medicine where high-resolution biomarker profiles are necessary[12]. Further, studies like those by Abasıyanık et al. have demonstrated the clinical impact of ultrasensitive digital assays by correlating cytokine levels with disease outcomes, such as predicting mortality in septic shock patients. This correlation highlights the potential for these assays in real-time clinical monitoring and decision-making[13]. Moreover, digital methods have been crucial in understanding immune responses and inflammatory conditions, as highly specific biomarker quantification provides insight into complex biological processes[5].

Despite the advances in sensitivity and multiplexing, a critical limitation remains: the lack of absolute quantification in many digital immunoassay platforms. While techniques like Simoa have achieved significant advances, they often rely on relative quantification, meaning that results are contingent on comparison with a standard curve or reference samples[7]. This dependence can introduce variability, particularly when analyzing complex or highly variable biological samples, or complicate measurement due to the complex and variable nature of reference production, especially for protein interaction quantitative references or protein conformation references. Platforms such as MOSAIC and dSimoa have improved sensitivity and sampling efficiency, allowing for the detection of rare biomarkers at attomolar concentrations, yet they also fall short in providing absolute molecular counts without external standards[6,8]. Similarly, proximity-based assays like PEA and PLA excel in multiplexing and detecting protein interactions but still primarily rely on relative measures rather than an absolute count of biomolecules[10]. The absence of absolute quantification remains a significant hurdle in immunoassay applications, particularly in translational research and clinical settings, where universal comparability and standardization across studies are essential. Achieving absolute quantification would enable consistent, reference-free measurements across different platforms and laboratories, providing a more robust foundation for biomarker validation, clinical diagnostics, and longitudinal studies[5,9]. In clinical scenarios, to predict outcomes in critical conditions, the ability to obtain absolute quantification could provide a more reliable metric for decision-making, improving the consistency of diagnostics across various patient populations and laboratories. The need for a true, reference-free quantification method is therefore one of the most pressing areas for innovation in the field, with the potential to bring unprecedented accuracy and comparability to proteomic measurements.

Results

Lossless, zero background detection principle - partitioning of single molecules, analytical limit of detection

We have pioneered an approach, termed *protein interaction coupling* (PICO[14,15]), architected to improve existing methods (for workflow Fig 1.a). PICO involves a binding and detection step. The binding step consists of the equilibrium binding of two DNA-labeled antibodies (antibody pair - ABP), which together define the target analyte. The detection step is based on the PCR amplification of these labels in compartments. This detection relies on identifying distribution differences of the antibodies alone, allowing for precise molecular counting using a novel principle based on detecting a biased Poisson distribution of antibodies induced by the presence of the antibody-bound analyte. For the sake of simplicity the term *couplex* is defined as the ternary complex constituted by the two antibodies and the target proteoform. The couplexes are quantified (see Fig 1.a for general dPCR concept see[16]) by a novel statistical model tailored to analyze data based on Poisson-distribution[17] called *compartment decouplexing*, or DX, (for the model see Appendix A). Utilizing this model, three pivotal parameters (concentration of couplexes, and of the two antibodies) are extracted that comprehensively characterize the individual reactions to derive the absolute couplex signal. Consequently, PICO readout manifests key analytical features, as corroborated by the low limit of absolute detection of DNA-based artificial couplexes (LOD=3 molecules per reaction) illustrated in Fig 1.b. Any antibody co-localizations, which are not a couplexes, are efficiently filtered out by the decouplexing model, which contributes to the digital enumeration of the signal. This clearly illustrated in Fig 1.b displaying a unit of slope and a Y-intercept at zero. However, it should be noted that the derived couplexes are probabilistic variables with inherent calculable variance, as detailed in Appendix A and attested by simulation data (Fig A1), which in turn influences the precision of the assay. Also, couplex values are normally distributed (Appendix A).

Theory of affinity of antibody independent absolute quantification

To derive the antibody K_d-independent absolute quantification of proteoform targets, we have formulated and analyzed an *ternary-equilibrium-based absolute quantification model* (i.e. AQ model) (Appendix B, see for

numerical analysis B2). We derived motivation from a range of models that have been utilized to study ternary binding in previous studies[18] (see other references in Appendix B), however our analysis is specific for solution phase ternary immunoassays and reveals implications for pioneering absolute quantitative measurements. According to analyses of AQ model in Appendix B, also see Fig 1.c, the model characterized as a non-bijective curve predicting two antigen concentrations for each measured couplex value. It is noteworthy that the dual readout effectively doubles the dynamic range achieving a dynamic range of five magnitudes routinely (Fig 1.f-g). At saturating concentrations of antibodies (Fig 1.e), according to the analysis the low side of the curve is negligibly influenced by the dissociation constant of antibodies (K_d), whereas the high side is exclusively dependent on antibody concentration, devoid of K_d influence (Fig B4.a-b). The model further exhibits a slope of unity (and minus unity) as a dual linear behavior in log-log representation, thereby enabling, additionally, facile ratio calculations for relative couplex quantification (Fig 1.c). Consequently, K_d-independent behavior in PICO assays is attainable at saturating antibody concentrations (Fig 2). Under these conditions, the concentration of couplexes equals with the concentration of the antigen on the low side, while the antigen concentration on the high-side can be directly inferred from the concentrations of antibodies and couplexes. In practical terms, the antigen concentrations of the model for both the low and high sides can be computed using an appropriate surrogate K_d. The analysis Fig 2 shows the precision of the absolute quantitative concentration of the analyte with a fixed antibody concentration while varying the surrogate K_d. The findings indicate that an appropriate choice of surrogate K_d can ensure significant precision across the entire range of complex concentrations regardless of true K_d. Based on the data presented in Fig 1.b, the decouplexing method yields molecularly precise readouts. The AQ model, under saturating conditions, accurately predicts absolute molar quantities of analytes, down to a few molecules. Consequently, it is important to note that the sensitivity of the PICO assay is primarily limited by the compartment size (i.e., the number of compartments), as compartmentalization of single molecules normally necessitates a dilution step, see also Figs B3 and C7.

Proof of absolute quantification

To validate the AQ model underlying the absolute quantitative PICO assay, a comprehensive set of experimental models was developed. Fig 1.d presents a both internally and externally verifiable experimental setup termed triangular PICO (3-cplex assay), in which three distinct PICO antibodies concurrently quantify the analyte. Noteworthy, that under saturating conditions, all three antibodies bind to the analyte simultaneously. As a verification, under saturating conditions, all three ABPs must yield equivalent absolute quantities internally. These internal measurements should also align with the concentration of an externally verified recombinant analyte standard. Fig 1.d shows the concept of the AQ verification experiments of rErbB2 (his-HER2) analyte under saturating condition with the verification of saturation (Fig 1.e), the calculated AQ plots of all three ABPs and all dilutions of analyte (Fig 1.f), linearity and dynamic range (Fig 1.g-h), and the derived absolute amounts under varied experimental setups (Fig 1.i). Similar AQ experiments using a recombinant polytag analyte (HIS-thioredoxin-STREP protein) described in C5. Both lines of experiments corroborated the validity of the AQ model, affirming that accurate single-molecular readouts are precisely interpreted through the AQ framework. Results also includes adjustments pertinent to labeling efficacy and other factors see Materials and Methods (and Appendix B).

Validation of PICO in cellular matrix and against external references

To extend applications beyond the analytical recombinant systems, we aimed to address the demonstration of minimal to negligible matrix effects that otherwise could introduce bias due to different assay contexts. In Fig 3, we present data employing the same set of ErbB2 triangular antibodies that were previously utilized and validated in analytical experiments, now in cellular context. Notably, the readings obtained using the anti-HIS tag antibody need to be consistently negative since the anti-HIS tag antibody lacks epitope on natural ErbB2 (Fig 3.b). These zero readings encompass the no-cell controls, an antibody only negative control (ABC), which expected to be zero, as well. Various dilutions of lysed BT474 and MCF7 cells measured with anti-HIS-tag result in zero couplexes. (Fig 3.c-d-e). The dataset not only demonstrates the absence of the background (ABC values) but also validates the presence of minimal to no matrix effects for challenging lysed cellular context (anti-HIS ABPs). Furthermore, according to Fig 3.g in lysed cellular context the spiked-in amount of rErbb2 was recapitulated. We, also, conducted an extensive AQ PICO measurement (n = 178), comparing results against a commercial ELISA, using BT474 and MCF7 cells with two different ErbB2 ABPs, also by different operators (Fig 3.f). Importantly, the absolute cellular amounts of natural ErbB2 measured were consistently in agreement within a given cell type, especially for MCF7, while at extreme high Erbb2 concentration values, in BT474, significantly differed, though with a low fold changes. To prove specificity of PICO regardless of the assay context, we conducted an ErbB2 spike-in experiment (Fig 3.g). In this experiment, quantified recombinant ErbB2 was added to lysed cells. All absolute quanties, including the amount of spiked-in rErbB2, and the measured natural ErbB2 amounts, were found to be accurate and summable, thus confirming the specificity of determining correct absolute amounts in PICO, irrespective of the formidable and chemically diverse environment of lysed cellular contexts.

PICO was compared to SIMOA [7], Fig C7, and Western blot (Fig 3.a, 4.a). SIMOA is showing comparable molar sensitivities (LODs are fM for SIMOA and 10s of fM for PICO, Fig C7.b) under conditions applying comparable number of beads and compartments, respectively, however, comparing them directly is challenging because of inherent differences. PICO uses a sample volume 15 times smaller, but if compensated for this, they exhibit equal sensitivity (≈2 fM). Additionally, PICO has a sensitivity-limiting dilution step before detection. Commercial dPCR instruments used for PICO have less compartments than the applied beads in SIMOA, which is a practical limit for sensitivity of PICO rendering it in the 100s of fM - pM range, however with hyperwelling (merging physical dPCR wells) (Fig C7) this boundary is permeable. Also, high-compartment-sized dPCR technologies are already on the horizon[19], offering theoretical attomolar sensitivities. Unlike PICO, SIMOA does

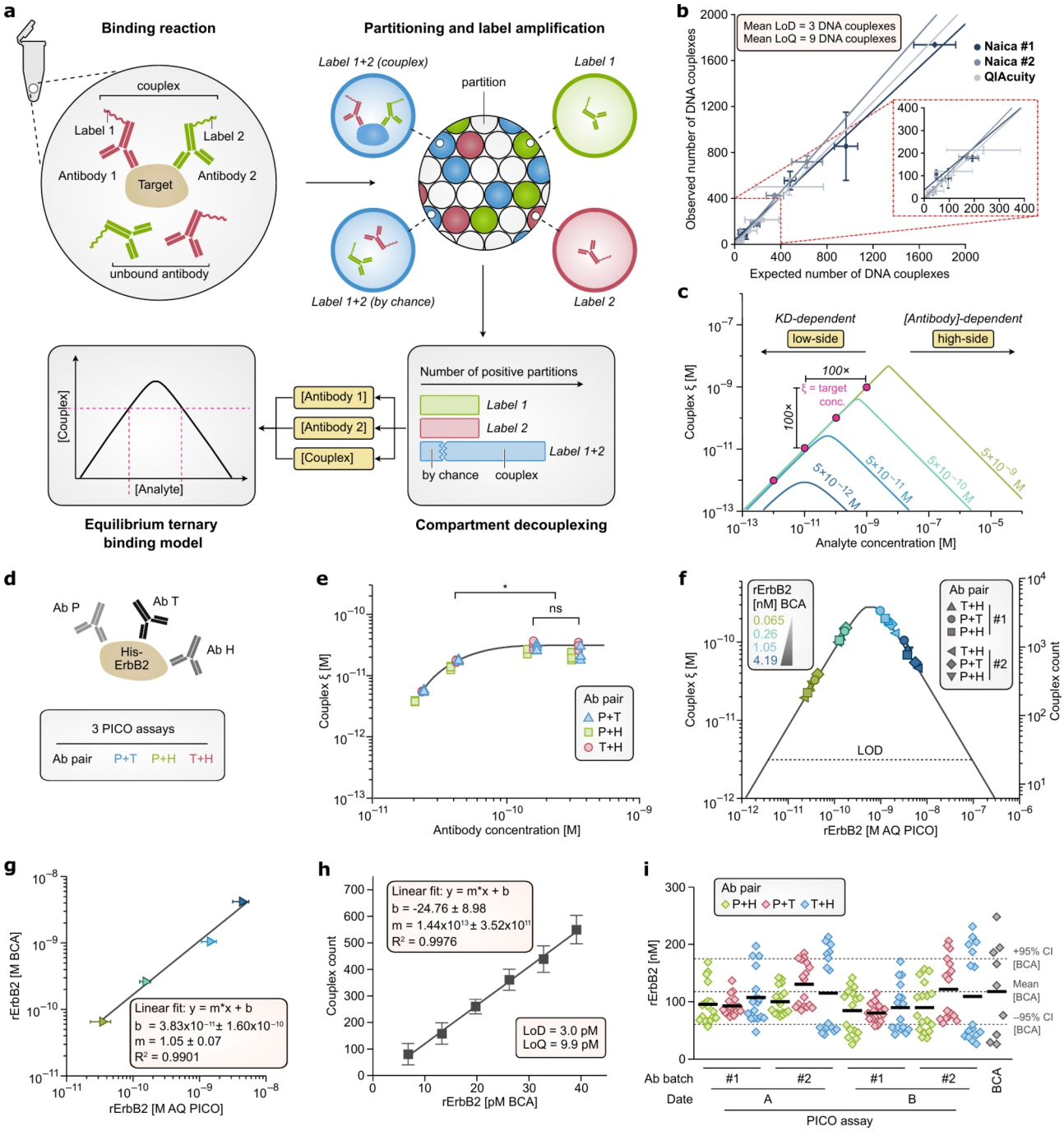
a
Binding reaction
couplex
Label 1
Label 2
Antibody 1
Target
Antibody 2
unbound antibody
Partitioning and label amplification
Label 1+2 (couplex)
partition
Label 1
Label 1+2 (by chance)
Label 2
[Couplex]
[Analyte]
[Antibody 1]
[Antibody 2]
[Couplex]
Number of positive partitions
Label 1
Label 2
Label 1+2
by chance
couplex
Equilibrium ternary binding model
Compartment decouplexing
b
Mean LoD = 3 DNA couplexes
Mean LoQ = 9 DNA couplexes
Naica #1
Naica #2
QIAcuity
Observed number of DNA couplexes
Expected number of DNA couplexes
c
KD-dependent
low-side
[Antibody]-dependent
high-side
100×
ξ = target conc.
100×
5×10⁻⁹ M
5×10⁻¹⁰ M
5×10⁻¹¹ M
5×10⁻¹² M
Couplex ξ [M]
Analyte concentration [M]
d
Ab P
Ab T
His-ErbB2
Ab H
3 PICO assays
Ab pair P+T P+H T+H
e
*
ns
Ab pair
P+T
P+H
T+H
Couplex ξ [M]
Antibody concentration [M]
f
rErbB2 [nM] BCA
0.065
0.26
1.05
4.19
Ab pair
T+H
P+T
P+H
#1
#2
LOD
Couplex ξ [M]
Couplex count
rErbB2 [M AQ PICO]
g
Linear fit: y = m*x + b
b = 3.83x10⁻¹¹± 1.60x10⁻¹⁰
m = 1.05 ± 0.07
R² = 0.9901
rErbB2 [M BCA]
rErbB2 [M AQ PICO]
h
Linear fit: y = m*x + b
b = -24.76 ± 8.98
m = 1.44x10¹³± 3.52x10¹¹
R² = 0.9976
LoD = 3.0 pM
LoQ = 9.9 pM
Couplex count
rErbB2 [pM BCA]
i
Ab pair
P+H P+T T+H
+95% CI [BCA]
Mean [BCA]
–95% CI [BCA]
rErbB2 [nM]
Ab batch
Date
#1
#2
#1
#2
BCA
A
B
PICO assay

◀**Fig. 1**. (**a**) The schematic workflow for absolute quantification. The PICO binding reaction described by the AQ model (Appendix B), and consists of the analyte and two amplifiable DNA label-conjugated antibodies under appropriate binding concentrations and conditions (D.5). After incubation the reaction is subsequently diluted according to the conditions required for a single-molecule digital PCR (dPCR) D.4. To provide inputs for the AQ model, the concentrations of couplexes and antibodies required are determined using the decouplexing model (Section A), ultimately yielding the absolute concentration of analyte. Additionally, the labeling efficiency is considered for antibody concentration correction (Section D.3). (**b**) Analytical PICO. Spiked-in versus observed number of artificial DNA couplexes applying the decouplexing model. The experimental details are in Method and Reagents D.6. The experiments were repeated on different devices as indicated. R^2 is larger than 0.99 in all cases, the slopes are 1.04 ± 0.39 for Qiacuity and 1.14 ± 0.15 for Naica, respectively, indicating 1-to-1 correspondence between spiked-in and measured amounts, showing lossless single-molecule counting. The average Y-intercept is -2 ± 10 couplex, indicating zero background. The mean analytical LOD of analytical PICO is 3 couplexes and the LOQ is 9 couplexes, based on the devised calculations of Wenzl et al.[34]. (**c**) The non-bijective calibration curve of the AQ model relates absolute analyte concentration (x-axis) to measured couplex molar concentration (ξ, y-axis) in the binding reaction. It demonstrates the influence of decreasing antibody concentrations. Under saturated conditions, for the three highest antibody concentrations, the antibody concentration and the K_d-dependence of ξ is eliminated. While on the high side, the analyte concentration is calculated from the antibody concentrations using the AQ model. See AQ model in Section B for more details. At saturation, the curves exhibit a 1-to-1 correspondence by definition, with a unity slope outside the peak region (see text and relative quantification B.2). An unknown concentration is measured by performing at least one dilution of the sample to determine the sidedness (low- or high-side) of the original sample. (**d**) Proof of absolute quantification. BCA (bicinchoninic acid) verified amount of recombinant ErbB2, as quantitative external reference, was assayed in a triangular PICO setup using trastuzumab (T), pertuzumab (P) and anti-HIS (H) antibodies (see Materials and Methods D.1 and D.5). In the triangular PICO concept, the three antibodies forming three ABPs, which quantitative, pair-wise PICO AQ results must equal (internal verification) if absolute quantitativity holds. (**e**) An isomolar (antigen) titration (D.5) was conducted at various concentrations of antibodies (13 pM, 40 pM, 120 pM, and 360 pM) with a fixed rErbB2 concentration of 40 pM. At the higher antibody concentrations, the generated number of couplexes did not significantly differ (Kruskal-Wallis ANOVA with Tukey's test, $p < 0.05$), indicating that a saturation concentration of the standard ABX = 500 pM suffices for all antibodies. (**f**) AQ (calibration) curve of recombinant ErbB2 (BCA verified). Symbols indicate different ABPs. The verified mean concentration of (all three) antibodies from the first batch is $5.3 \times 10^{-10} \pm 9.2 \times 10^{-11}$ M (n=138) and for the second batch $5.6 \times 10^{-10} \pm 6.1 \times 10^{-11}$ M (n=138), saturating concentration. The assay carried out using two different batches of antibodies (#1 and #2), each marker representing the mean of 6 replicates and with standard deviations are shown (mainly imperceptible), n=216. The dotted line denotes the LOD of measurement (20 couplexes, LOD 3 pM). (**g**) BCA reference vs. AQ PICO (data from Fig 1.f see also c.). A regression line has a slope of 1.05 ± 0.07, intercept 38 ± 160 pM and $R^2 = 0.99$ with $n = 216$, confirms the linearity of the AQ model involving both sides of the curve. (**h**) The relationship between the measured number of couplexes and the reference (BCA) values for the rErbB2 analyte, within close vicinity of the limit of detection (LOD), at 7 pM, 13 pM, 20 pM, 26 pM, 33 pM and 39 pM of rErbB2, respectively. LOD was 30 pM and LOQ 10 pM. Slope m = 14 ± 0.35, y-axis intersection $b = -24 \pm 9$, $R^2 = 0.99$, $n = 36$. (**i**) Distribution of the measured absolute amounts of the rErbB2 quantitative reference normalised for dilution (see also c.). Two different time point, two different batches of antibodies, three ABPs and four dilution of of the analyte. The BCA quantified reference indicated (118 ± 87 nM) with 95% confidence intervals. Values from left to right are 95 ± 33 nM, 92 ± 16 nM, 107 ± 45 nM, 99 ± 23 nM, 130 ± 38 nM, 115 ± 69 nM, 84 ± 39 nM, 80 ± 15 nM, 89 ± 40 nM, 89 ± 40 nM, 121 ± 52 nM and 109 ± 79 nM stock concentration, respectively. ANOVA shows no significant differences observed in terms of ABPs, assay dates, and PICO compared to BCA ($F(12,202) = 1.77$, p-value $= 0.05$, $n = 211$). These findings substantiate the absolute quantitative measurement of recombinant ErbB2, demonstrating lossless molecular counting, negligible background, and pronounced linearity over 3.5 log dynamic range.

not function as a single-molecule counting assay, as verified and evident from the absolute amounts detected (see LOD [#molecules] in Fig C7.c), and it is not background free [7]. Fig 3.e shows the cellular LOD of ERbb2 PICO (17 ± 16 cells for BT474, 1.6×10^6 ErbB2 copies per cell, and 980 ± 860 cells for MCF7, 1.2×10^4 ErbB2 copies per cell) against Western blotting, Fig 3.a, (LOD of 40,000 cells for BT474) clearly demonstrating a sensitivity increase by a factor of more than 2000 times. PICO, a liquid phase assay, has no lower assay volume limit, allowing for adjustment of binding conditions through volume downscaling. This reduction in volume decreases antibody quantities at the same concentration, enabling a significant reduction in the extent of dilution, and pushing the assay's absolute sensitivity from the attomole regime down to the low zeptomole level, allowing detection of just a few molecules. This adaptability allows PICO to achieve sensitivities down to scope a single-cell while maintaining it lossless absolute quantitative performance (unpublished data).

Multiplex PICO measuring cellular stoichiometry with high precision

Based on the proven absolute quantitative PICO, a novel 8-plex PICO assay was designed, which aimed to partly replicate previously reported complex pathway studies[20], and including many proteoforms, extending the PICO assay toward highly parallel regimes. Fig 4 presents an 8-plex, split-readout dPCR-based PICO assay, with the split readout of S6K1, p4EBP1 and ErbB2, ErbB3, ErbB2:ErbB3 interaction, respectively (Fig 4.d) including protein,

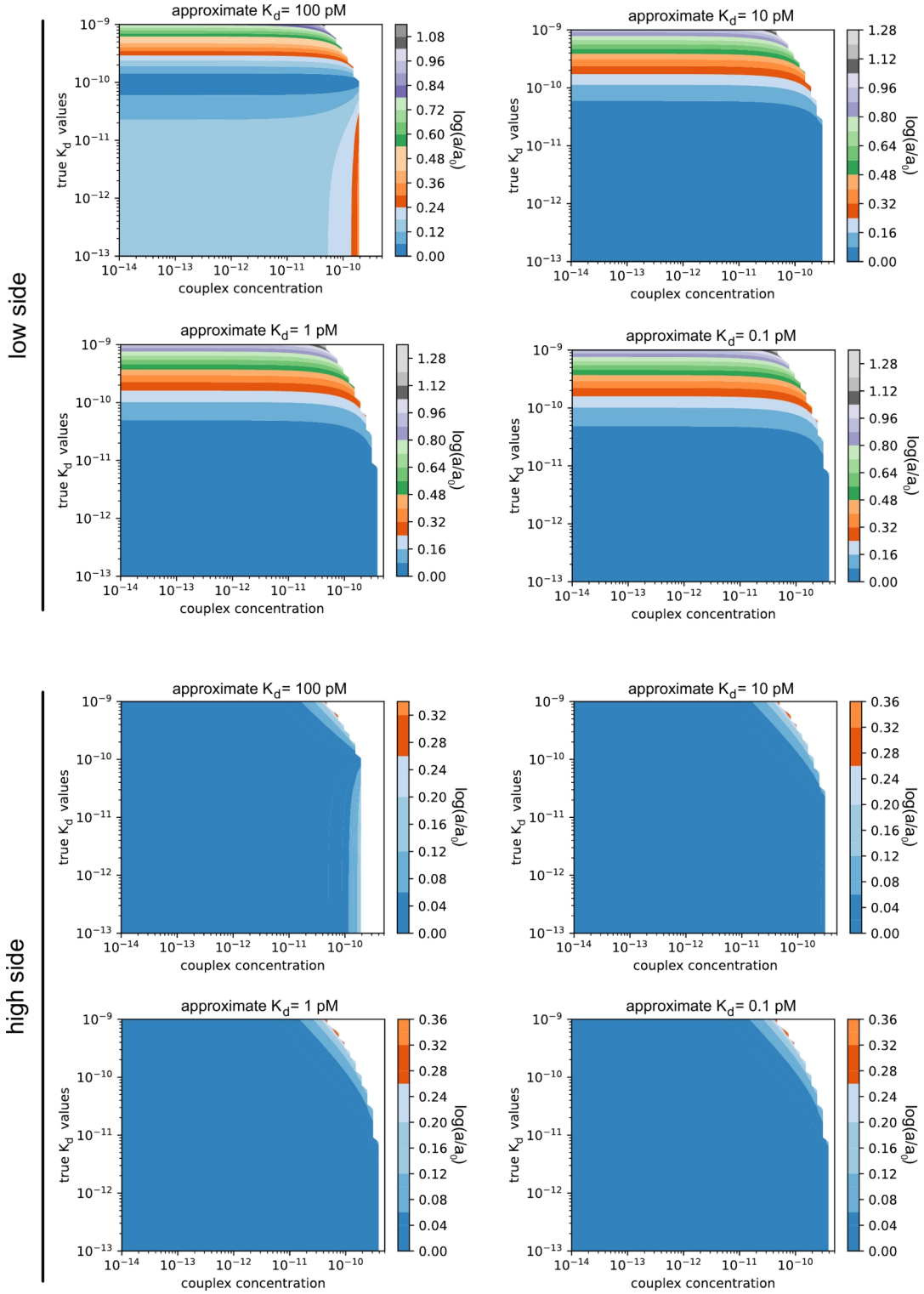
low side
high side
approximate K_d= 100 pM
approximate K_d= 10 pM
approximate K_d= 1 pM
approximate K_d= 0.1 pM
true K_d values
couplex concentration
log(a/a$_0$)

◀**Fig. 2**. Relative precision of absolute concentration of analyte assuming 5.0×10^{-10} M antibody concentration while the surrogate K_d of antibodies are varied. X-axis is the concentration of couplexes, while Y-axis represents the true K_d value. The color coded values are the logarithm of the ratio of the calculated and real a_0. The upper graphs show the low side while the bottom graph represent the high side of the curve, $\log_{10}(2) = 0.3$, which indicates the two-fold difference, was taken as an precision threshold. Based on this analysis, it is evident that the choice of a surrogate K_d is flexible, provided it exceeds the saturation concentration of the given antibody. When using a surrogate K_d of 10 pM or lower (also a safe default is 50 pM), the low-side exhibits remarkable precision, particularly when the true K_d falls below 200 pM. It's noteworthy that the peak region, situated at the right edge of the graph and neighbored by a mathematically inapplicable white area, maintains precision akin to the entire curve on the low side or only nuancely influenced by the couplex concentration on the high side. Therefore, using the the model of $p = (b_{01}, b_{02}, \xi)$ even the peak region attains high precision using a proper surrogate K_d, however to avoid K_d above the threshold it is recommended conducting IT experiments to ensure high precision.

phosphoprotein and interaction targets. The assay detects 6 targets (the ErbB2:ErbB3 interaction measured with two different ABPs), and 6 BAB pairs (bystander antibody controls) i.e. confirmatory to zero readouts (Fig 4.e-f). Combinatorial multiplexing (cplex) exerts exceptional control over PICO reactions. The 8-plex split-readout PICO, taking into account the cell dilutions as distinct samples, includes 18 non-target BAB readings, and 12 no-cell negative controls, which are essential for leveraging dPCR clustering biases (see Methods). Furthermore, there are 18 target readouts. As the purposely applied pertuzumab cannot bind to ErbB2:ErbB3 complexes[21] providing a unique opportunity to confirm the zero PPI readings by comparing them to trastuzumab ABPs, both of them even based on two different ABPs readouts (Fig 4.f). Furthermore, the two trastuzumab-based readouts are non-significatly different (Fig 4.i) along all conditions. Nevertheless, the functionality of pertuzumab is intact per ErbB2 readouts (Fig 4.g-h). Small, down to 1.33-fold, and large fold changes are precisely measurable between treatments (Fig 4.g-h). The absolute quantitative results enable unrestricted comparisons revealing the quantitative stoichiometry of protein complexes and phosphoproteins, even between cells, especially for p4EBP1 (Fig 4.c) and ErbB proteins (Fig 4.g-h), elegantly proposing the rate-limiting nature of ErbB3 expression in the ErbB2:ErbB3 complex formation in MCF7 cells. Regarding dactolisib treatment of MCF7 (low ErbB2) and BT474 (high ErbB2) cells, 8-plex PICO recapitulates earlier[20] findings of increased ErbB2 and ErbB3 expression, however, while ErbB2:ErbB3 is confirmatively increased in MCF7 cells as well, in BT474 it is reduced to an undetectable level, falling below the limit of detection (LOD) of 180 molecules per cell. In contrast, untreated BT474 cells exhibited detectable ErbB2:ErbB3 interaction.

Discussion

Despite many available immunoassays (IA)[22–24] some improvements are still expected. The ever-more-capable IAs (Appendix C, Table C1) have achieved very high sensitivities, in both molar, SIMOA, NuELISA and PEA[7,25,26], and absolute terms[27], and reached high parallelism OLink[10] and SOMAmers[28]), however, one feature is still missing - a truly quantitative reference-free IA for the absolute, and universally comparable quantification of the analytes. Besides evident practical reasons, absolute quantification of proteoforms is a must for highly parallel cellular stoichiometry[29] waiting to set out to understand intricate cellular workings and exploring maybe just stoichiometrically different views with consequent functional differences[30]; recently, structural studies have opened up views on the diverse proteomic and interatomic landscape and, naturally, on the intriguing stoichiometrics of these diversities[31]. In this context, PICO introduces new paradigms, comprising a compartmentalized, homogeneous, single-molecule assay using a new lossless signal generation principle, which robustly achieves a limit of detection (LOD) of a few or practically zero molecules per reaction, limited only by unavoidable Poisson-based stochasticity. Through its unique physical assay principle of partitioning, read out by decoupexling, and its inherently separate binding and detection steps, PICO stands alone in achieving zero background. The absolute signal is mathematically described introducing practically attainable theoretical chemistry for IAs. PICO achieves absolute, lossless quantification of target proteoforms through (1) the single molecule sensitivity of the applied compartmentalized PCR detection and the physically compartmentalized signal generation (dPCR). Additionally (2) the absence of background-contributing side reactions guarantees (3) zero background signal borrowed from the absolute, digital counting of dPCR. Moreover, it is (4) independent of antibody dissociation constants (K_d) by choosing carefully orchestrated chemical conditions, and importantly, PICO is (5) homogeneous ensuring a robust, lossless process, without washing steps. The (6) high specificity of PICO is defined by two antibodies conjugated to amplifiable DNA labels, strictly binding of both asserts the signal. Thereby drawing conceptual parallels to other bi-component assays that are predominantly enzyme-label reliant, however, in the case of PICO, (7) under stringent, aspecific binding suppressive conditions. The PICO readout are not being restricted to given, cognate antibody pair, as signals between any antibody pairs can be read out. Combinatorial multiplexing (cplex) (8), exemplified here as triangular, quadratic (three and six ABPs). The number of ABPs that can be analyzed has recently reached to 12, with the potential to reach at least a hundred in the foreseeable future. Validation experiments, including internal and external verifications, confirm the reliability of absolute quantitative PICO across various experimental setups, including cellular contexts, plus demonstrating unique features, like combinatorial multiplexing (cplex) exemplified here by triangular, quadratic PICO assays Fig 1.d and 8-plex split Fig C5.e. These higher-order cplex assays facilitates complex readout of proteoforms e.g. complex protein interactions and concurrently the involved interacting proteins are measured (for six ABPs, Fig 4), enabling self-confirming multiple measurements on the very same target molecule, and an array of negative (expecting zero signal) control reactions (using BABs or just between non cognate antibodies)

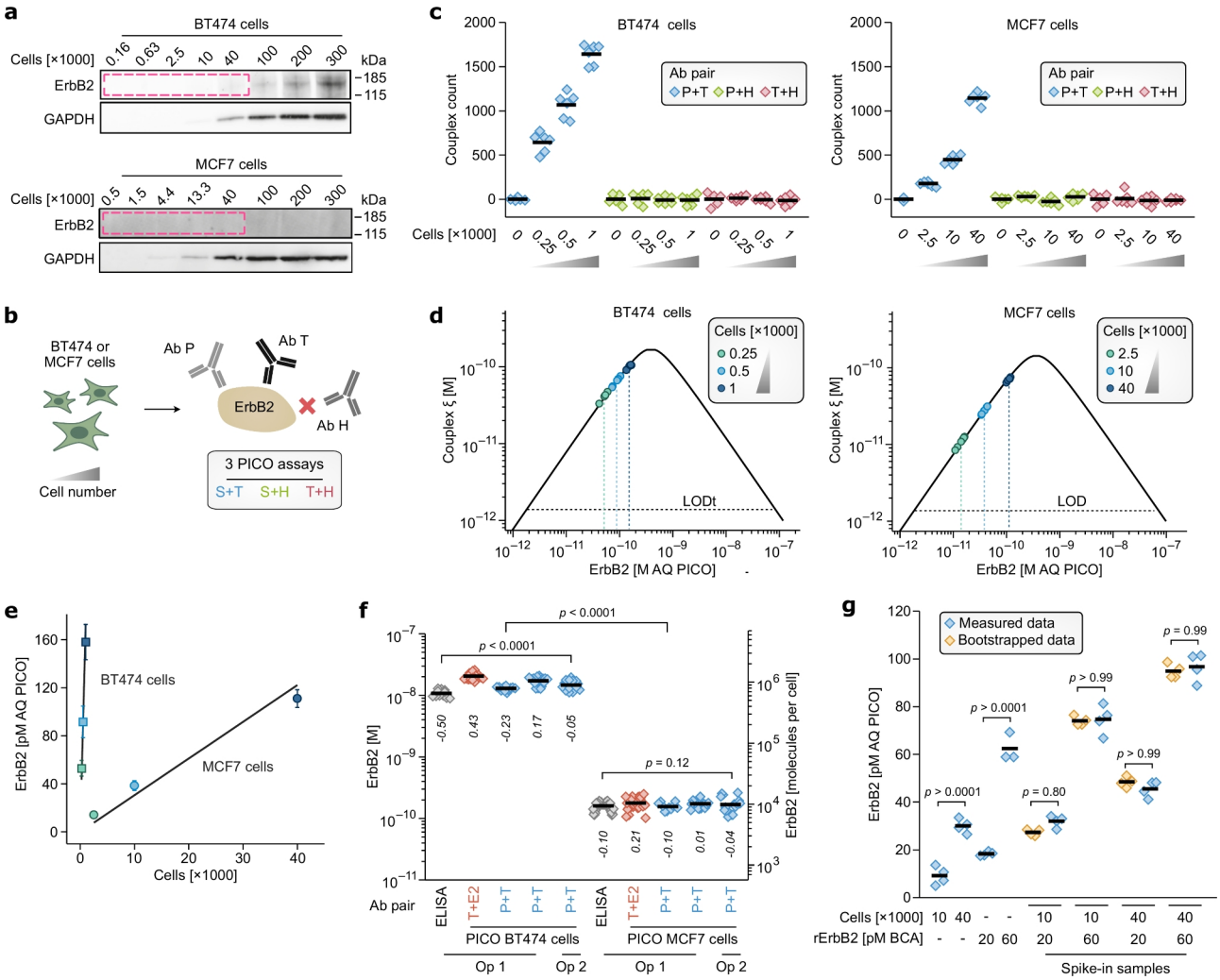

exerting strict control over the entire multiplex reaction network. PICO enables even structural studies, i.e. the therapeutic antibody of ErbB2, pertuzumab, known having epitope on the interaction surface[21] rendering the ErbB2:ErbB3 interaction signal to be zero, while trastuzumab still detects the interaction absolute quantitatively. Compared to existing techniques like SIMOA[32] and Western blotting, PICO exhibits noticeable advantages, especially evident in cellular LODs, outperforming Western's sensitivity. dSIMOA is reported to enable absolute quantification; however, without access to the technology, we were unable to demonstrate this in our work. Nevertheless, according to the published data[7], the limit of detection (LOD) for dSIMOA is estimated to be a few thousand molecules, which appears to require an external reference for accurate molar corrections. Upon dactolisib treatment, the increase of ErbB2:ErbB3 interaction was recapitulated[20] in the breast cancer cell line MCF7 using 8-plex detecting down to 180 proteins in cells Fig 4 demonstrating multiplexity, combinatorial multiplexing, the detection of an array of proteoforms, self-confirmation, structural hindering and strict control of specificity. Nevertheless, PICO is homogeneous and solid-phase-free unlike ELISA-based concepts (i.e.[27,7] and[28]), allowing the adaptability of the assay to ultra-low volumes and allowing PICO to achieve sensitivities in absolute terms down to the scope of a single cell, i.e. detection of zeptomoles were demonstrated in single-cells, while maintaining its absolute quantitative, lossless performance (using a 12 nL PICO reactions, CSHL Single Cell Analyses, Nov 8 - 11, 2023, manuscript in preparation). While others fail to show negligible background, which in turn hampering quantification at the single cell level[33]. The data also demonstrate PICO endurance against matrix effects and exhibiting high specificity Fig 3.c and g., which was further underlined by absolute detection of rErbB2 in spiked-in whole blood (unpublished) or demonstrating zero signal indicating mutually exclusive binding (see above Fig 4) and using anti-p4EBP1 and anti-4EBP1 Abs targeting the same epitope, unpublished). In conclusion, PICO has enormous potential, offering versatile, standardized, precise measurements of proteins, providing insights into the physiologically relevant stoichiometry of disease-related cellular processes, even revealing structural intricacies and hence facilitating the development of therapeutic agents [3].

◀**Fig. 3**. (**a**) Western blotting involved loading varying cell quantities of BT474 and MCF7 cells as indicated, followed by immunodetection using trastuzumab (anti-ErbB2) and anti-GAPDH antibodies as loading control (detailed in Material and Methods, Section D.8). For BT474 (ErbB2 over-expressing breast cancer cellline) the ErbB2 signal diminished to an undetectable level at approximately 40,000 cells per lane. Notably, ErbB2 expression in MCF7 cells was scarcely detectable even at 300,000 cells, while the loading controls are comparable. BT474 cells express 1,940,000 ERbB2 proteins per cell (qFACS)[35], while MCF7 exhibits approximately 100-fold lower expression (Western)[36]. Considering a limit of detection (LOD) at 40,000 cells for BT474, MCF7 falls below the LOD of Western at 300,000 cells. (**b**) ERbB2 triangular PICO assay with bystander antibody. See also Fig 1.d, note that Ab H was used here as a bystander antibody - BAB, as an internal negative control, as natural ErbB2 has no HIS-tag. (**c**) Absolute number of couplexes measured of ErbB2 PICO using different number of lysed BT474 and MCF7 cells (each 6 parallels), as indicated, and ABPs, all assayed at $\lambda = 0.15$, as described in Material and Methods (D.5). An analyte-free negative control was used, and expected to be zero. Data is normally distributed (Shapiro-Wilk, $p > 0.1$, $n = 144$), the cell measurements of P+T ABP are all significantly different from zero (t-test, $p < 0.001$, $n = 36$), while BAB pairs are not significantly different from zero (t-test, $p > 0.1$, $n = 108$), means are indicated. The bystander antibody (BAB) measuring unspecific binding, the consistently zero BAB signals confirm zero background. (**d**) AQ curves of BT474 and MCF7 of ErbB2 PICO based on Fig.**c** data. The Y-axis represents the concentration of couplexes, and the X-axis denotes the absolute molar concentration of the analyte in the binding reaction. The mean concentration of the antibodies of T and P for the BT474 assay is $3.6 \times 10^{-10} \pm 4.5 \times 10^{-11}$ M (n=46) and for the MCF7 $3.3 \times 10^{-10} \pm 3.6 \times 10^{-11}$ M (n=40), saturating conditions. The calculated absolute concentrations effectively replicate the cell dilution series (indicated in the legend, see also Fig.**e**), and yielding estimates of $8.9 \times 10^5 \pm 1.5 \times 10^5$ ErbB2 per cell for BT474 and $9.9 \times 10^3 \pm 3.2 \times 10^3$ ErbB2 per cell for MCF7, corresponding a $90\times$ of relative expression difference, confirming previous findings[36]. The slight departure of BT474 expression form qFACS data ($\sim 0.45\times$) is explained by biological variability or reproducibility problems (for qFACS[37]), also PICO is highly consistent between experiments, and with ELISA, see also (Fig.3.f). (**e**) Absolute concentration vs. cell number of data Fig.**c**. The LOD calculation was conducted according to Wenzl et al.[34],and a LOD of 17 ± 16 BT474 cells and 980 ± 860 MCF7 cells were determined, respectively. Similarly, LOQs were 75 ± 53 BT474 cells and 4264 ± 2826 MCF7 cells, BT474 $R^2 = 0.985$, MCF7 $R^2 = 0.958$. (**f**) The reproducibility of PICO. ErbB2 proteins of BT474 and MCF7 cells were measured with PICO, including varied of ABPs and operators and verified against ELISA. The double Y-axis represent ErbB2 concentrations (in the binding reaction) and proteins per cell. Log2 fold differences were calculated as (sample mean) / (group mean), and also indicated. All (PICO) average copy numbers per cell of ErbB2 were 1×10^6 ($\pm 2.1 \times 10^5$), and 1.1×10^4 ($\pm 3 \times 10^3$) ($n = 178$), for BT474 and MCF7, respectively. BT474 cells expressed approximately 96 (± 25) times more ErbB2 than MCF7 cells, a significant difference (F(9,220)=941.64, p-value<0.0001, n=229). ANOVA revealed no statistical difference between MCF7 samples (F(4, 135)=1.86, p-value $= 0.121$, n=139), while BT474 cells exhibited significant differences (F(4,85)=53.03, p-value < 0.0001, n=89), albeit with minimal deviation ($CV = 20.56\%$) and low fold differences, attributable to biological variations. ELISA measured an ErbB2 expression per cell $6.5 \times 10^5 \pm 8.3 \times 10^4$, 0.7 times less than average PICO data, $p = 0.0026$, $n = 66$, and $9.5 \times 10^3 \pm 1.6 \times 10^3$, 1.1 times less then PICO, $p = 0.19$, $n = 118$, for BT474 and MCF7, respectively. The individual molar ErbB2 of each group from left to right are 10 (± 1) nM, 20 (± 2) nM, 13 (± 1) nM, 17 (± 2) nM, 14 (± 2) nM, 157 (± 26) pM, 194 (± 56) pM, 157 (± 22) pM, 169 (± 40) pM, 164 (± 53) pM. Altogether PICO showed high precision and reproducibility, especially for MCF7 cells, BT474 has higher ErbB2 expression per cell and consequently more effected with sampling errors of cell counting.**g**. The specificity of PICO. An absolute quantitative spike-in experiment was carried using two dilutions of MCF7 cells (10,000 and 40,000 cells, representing the theoretical concentrations of 39.3, and 157.5 pM, respectively) and rErbB2 protein (60 and 20 pM). Samples were as indicated ($n = 4$), and were compared to bootstrapped values. ANOVA were applied to compare bootstrapped combinations of MCF7 and rErbB2 concentrations demonstrating no significant differences ($p < 0.05$) in all comparisons. The spike-in experiment demonstrates robust specificity, allowing unbiased measurement of rErbB2 levels in the presence of endogenous ErbB2 and lysed cell material, maintaining concentration additivity.

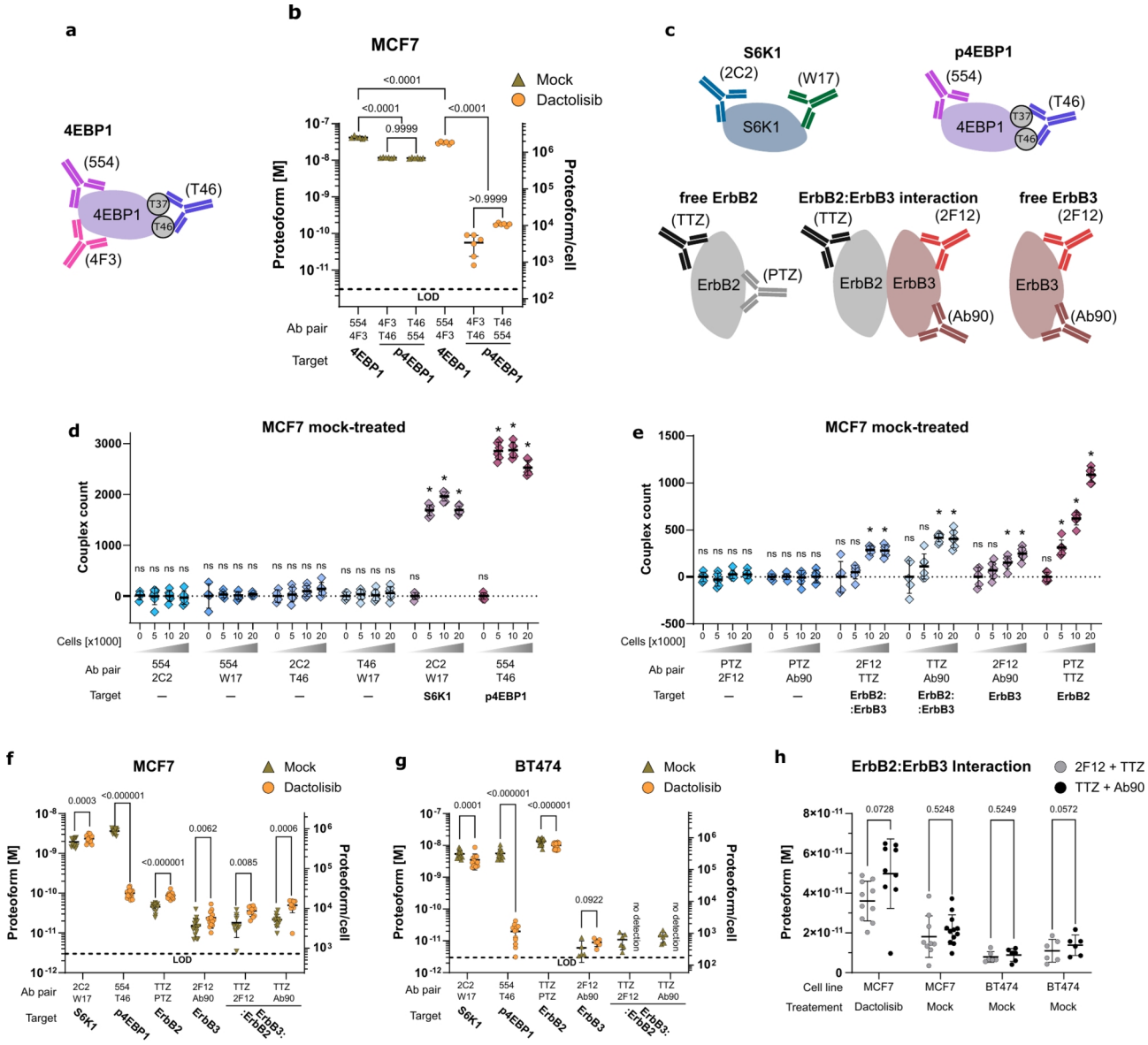
a
4EBP1
(554)
(T46)
T37
T46
(4F3)
b
MCF7
Mock
Dactolisib
<0.0001
<0.0001
<0.0001
0.9999
>0.9999
Proteoform [M]
Proteoform/cell
LOD
Ab pair
Target
4EBP1
p4EBP1
c
S6K1
(2C2)
(W17)
p4EBP1
(554)
(T46)
free ErbB2
(TTZ)
(PTZ)
ErbB2:ErbB3 interaction
(2F12)
free ErbB3
(Ab90)
d
MCF7 mock-treated
Couplex count
Cells [x1000]
Ab pair
Target
S6K1
p4EBP1
e
MCF7 mock-treated
Couplex count
ErbB2:ErbB3
ErbB3
ErbB2
f
MCF7
Mock
Dactolisib
0.0003
<0.000001
<0.000001
0.0062
0.0085
0.0006
g
BT474
Mock
Dactolisib
0.0001
<0.000001
<0.000001
0.0922
no detection
h
ErbB2:ErbB3 Interaction
2F12 + TTZ
TTZ + Ab90
0.0728
0.5248
0.5249
0.0572
Cell line
Treatement
MCF7
BT474
Dactolisib
Mock

◀**Fig. 4**. 8-plex PICO assay detecting different proteoforms. (**a**) Triangular detection of 4EBP1 and its phosphorylation. Note that the redundant absolute quantification of 4EBP1 phosphorylation (measured by two ABP). (**b**) Detection of 4EBP1 protein and its T37-T46 phosphorylation using mock and dactolisib-treated MCF7 cells. After treatment 40k MCF7 cells were lysed and PICO absolute quantified. The y-axis is in molar concentration, while the right axis is proteoforms per cell, the LOD indicated. The mean number of proteoforms per cell (ppc), from left to right, are 2530000 ± 220000 ppc, 707000 ± 21000 ppc, 694000 ± 31000 ppc, 1810000.00 ± 90000 ppc, 3400 ± 2200 ppc, 10700 ± 700 ppc. Based on ANOVA ($F(5, 30) = 643.0$, $p < 0.0001$, $n = 36$), dactolisib significantly perturbs both protein and phosphorylation levels (both $p < 0.0001$, $n = 12$) the latter showing a significant difference in phosphorylation (27% versus 0.4%). 4EBP1 phosphorylation as detected by the two different ABPs showed no significant difference between mock ($p = 0.9999$, $n = 12$) and dactolisib-treated ($p > 0.9999$, $n = 12$) MCF7 cells demonstrating concordant absolute quantitative results. (**c**) Depictions of PICO assay used for the detection of the cytosolic protein S6K1 and p4EBP1 along with the detection of ErbB2, ErbB3, and ErbB2:ErbB3 interaction. The 8 antibodies were concurrently applied (8-plex PICO), however, detected by two different amplification primer pairs in separate dPCR reactions, S6K1, 4EBP1-phosphorylation and ErbB2, ErbB3, respectively. Note the inability of pertuzumab to bind to the interacting protein complex. (**d,e**) Couplex counts per dPCR reactions of 8-plex PICO using 0, 5000, 10000, or 20000 lysed MCF7 cells (each 6 replicates), ABPs are indicated, normalised and λ-corrected values (see methods). All antibodies were applied in parallel see (d), (e) S6K1 and p4EBP1, ErbB2 and (f) ErbB2, ErbB3 and ErbB2:ErbB3 interaction. The asterisk (*) indicates a p-value of less than 0.05. No sign indicates non-significant difference from zero ((e) - normality test Shapiro-Wilk test $p = 0.18839$, $n = 91$, two-sided one-sample t-test $t(90) = 1.62542$, $p = 0.10757$, $n = 91$; (f) - normality test Shapiro-Wilk test $p = 0.11861$, $n = 66$, two-sided one-sample $t(65) = 0.21725$, $p = 0.82869$, $n = 66$). (**f**) Mock or dactolisib-treated MCF7 cells (20k cells, low ErbB2 expression) were PICO absolute qualified using the 8-plex PICO assay described above (d), all comparisons are in mock-dactolisb order. S6K1 levels were marginally, but significantly different between mock and dactolisib treatments (468,000 ± 112,000 ppc and 567,000 ± 128,000 ppc, respectively) indicating high precision, but presumably no or minimal biological significance ($t(11) = 4.845$, $q = 0.000347$, $n = 24$). The pronounced and expected effects of dactolisib treatment on p4EBP1 were confirmed (875,000 ± 130,000 ppc and 24,200 ± 5,700 ppc, respectively, 36-fold difference, $t(10) = 20.54$, $q < 0.000001$, $n = 29$). Note that the level of p4EBP1 is susceptible to variations in culturing conditions. There was an expected, known difference in ErbB3 level, confirming literature (see main text) having 3,670 ± 1,980ppc and 5,810 ± 2,640 ppc, respectively, a 1.6-fold increase, $t(13) = 2.789$, $q = 0.006206$, $n = 32$. ErbB2 levels were also significantly different (10,940 ± 2,160 ppc and 21,100 ± 3,400 ppc, respectively, an 1.9-fold increase, $t(17) = 11.3$, $q < 0.000001$, $n = 36$). ErbB2:ErbB3 interaction was significant between treatments, however, consistent between the two antibody pairs TTZ-2F12 and TTZ-Ab90, respectively, having 4,370 ± 2,520 ppc and 8,670 ± 2,400 ppc, a 2-fold increase, $t(6) = 2.959$, $q = 0.008528$, $n = 19$ and 5,200 ± 1,810 ppc and 12,000 ± 4,200 ppc, an 2.3-fold increase, $t(8) = 4.848$, $q = 0.000644$, $n = 21$. In mock-treated MCF7 cells, approximately 44% of the ErbB2 protein engages in interaction with ErbB3. In contrast, treatment of cells with dactolisib induces a slight increase in this interaction, in line with the literature, resulting in a percentage of 49%, and underlines PICO's ability to detect such subtle changes. Interestingly, ErbB3 appears to be present in a limiting quantity under both mock and dactolisib conditions, as evidenced by the observation that nearly 100% of the protein interacts with ErbB2. (**g**) Mock or dactolisib-treated BT474 cells (40k cells, high ErbB2 expression) were PICO absolute qualified using the 8-plex PICO assay described above (d), all comparisons are in mock-dactolisb order. S6K1 levels were different, having 326,000 ± 95300 and 193,000 ± 60,700 ppc, $t(11) = 5.91$, $q = 0.000034$, $n = 24$, confirming precision, but marginal changes. p4EBP1 levels were consistent with the dactolisib treatment, 337,000 ± 125,000 and 1,190 ± 716 ppc, $t(11) = 9.32$, $q < 0.000001$, $n = 24$ exhibiting a high sensitivity to dactolisb and shows 283-fold phosphorylation difference. ErbB2 levels, contrary to MCF7 data, show a decrease of ErbB2 level upon dactolisib treatment, 808,000 ± 177,000 and 604,000 ± 128,000 ppc, a 1.33-fold decrease, $t(17) = 9.20$, $q < 0.000001$, $n = 36$. While ErbB3 protein levels were highly concordant with MCF7, having 312 ± 244 and 541 ± 142 ppc, an 1.7-fold increase, ($t(4) = 2.20$, $q = 0.023303$, $n = 12$). Nevertheless, ErbB2:ErbB3 interaction was only detectable in mock-treated cells, having concordant, non-significantly (see below) different levels with the TTZ- 2F12 and TTZ-Ab90 ABPs and was 662 ± 343 and 831 ± 311 ppc, respectively, the LOD was 200 ppc. In dactolisib-treated BT474 cells, the ErbB2:ErbB3 interaction is extremely low or absent, as evident from the data. While, in mock-treated cells, approximately 0.09% of ErbB2 interacts with ErbB3, while nearly 100% of ErbB3 engages in interaction with ErbB2, replicating its rate-limiting behaviour seen in MCF7 cells. (**h**) Highly concordant results between TTZ-2F12 and TTZ-Ab90 ABPs detecting the ErbB2:ErbB3 interaction from left to right are $t(7) = 2.588$, $q = 0.0728$, $n = 19$; $t(8) = 0.8282$, $q = 0.524873$, $n = 21$; $t(5) = 0.6921$, $q = 0.524873$, $n = 12$; $t(5) = 3.690$, $q = 0.05715$, $n = 12$, demonstrating the self-confirming applicability of such parallel measurement.

Data availability.

Additional data of the figures is on Figshare https://doi.org/10.6084/m9.figshare.25736883.v2. The figure data files are named according to the corresponding figure/subfigure (e.g., Fig 1 b.xlsx). The code used for decouplexing and absolute quantitative analysis is available on GitHub https://github.com/Actome-External/PICO_Analysis. Access is available from the corresponding author.

Received: 3 May 2024; Accepted: 18 February 2025
Published online: 01 March 2025

References

1. Muñoz, J. & Heck, A. J. R. From the human genome to the human proteome. *Angewandte Chemie International Edition* **53**, 10864–10866 (2014).
2. Mir, R.A., Shafi, S.M. & Zargar, S.M. *Analysis of proteomes-III* (Elsevier, 2023).
3. Calderón-Celis, F., Encinar, J. R. & Sanz-Medel, A. Standardization approaches in absolute quantitative proteomics with mass spectrometry. *Mass Spectrometry Reviews* **37**, 715–737 (2017).
4. Sanz-Medel, A., Montes-Bayón, M., del Rosario Fernández de la Campa, M., Encinar, J.R. & Bettmer, J. Elemental mass spectrometry for quantitative proteomics. *Analytical and Bioanalytical Chemistry* **390**, 3–16 (2007).
5. Cohen, L. et al. Single molecule protein detection with attomolar sensitivity using droplet digital enzyme-linked immunosorbent assay. *ACS Nano* **14**, 9491–9501 (2020).
6. Wu, C., Garden, P. M. & Walt, D. R. Ultrasensitive detection of attomolar protein concentrations by dropcast single molecule assays. *Journal of the American Chemical Society* **142**, 12314–12323 (2020).
7. Wilson, D. H. et al. The simoa hd-1 analyzer: A novel fully automated digital immunoassay analyzer with single-molecule sensitivity and multiplexing. *SLAS Technology* **21**, 533–547 (2016).
8. Wu, C., Dougan, T. J. & Walt, D. R. High-throughput, high-multiplex digital protein detection with attomolar sensitivity. *ACS Nano* **16**, 1025–1035 (2022).
9. Byrnes, S. A. et al. Wash-free, digital immunoassay in polydisperse droplets. *Analytical Chemistry* **92**, 3535–3543 (2020).
10. Wik, L. et al. Proximity extension assay in combination with next-generation sequencing for high-throughput proteome-wide analysis. *Molecular & Cellular Proteomics* **20**, 100168 (2021).
11. Schallmeiner, E. et al. Sensitive protein detection via triple-binder proximity ligation assays. *Nature Methods* **4**, 135–137 (2007).
12. Darmanis, S. et al. Proteinseq: High-performance proteomic analyses by proximity ligation and next generation sequencing. *PLoS ONE* **6**, e25583 (2011).
13. Abasıyanık, M. F. *et al.* Ultrasensitive digital quantification of cytokines and bacteria predicts septic shock outcomes. *Nature Communications* **11**, 2607 (2020).
14. Karakus, U. et al. MHC class II proteins mediate cross-species entry of bat influenza viruses. *Nature* **567**, 109–112 (2019).
15. Gross, T. *et al.* Characterization of crispr/cas9 rankl knockout mesenchymal stem cell clones based on single-cell printing technology and emulsion coupling assay as a low-cellularity workflow for single-cell cloning. *PLoS ONE* e0238330 (2021).
16. Quan, P.-L., Sauzade, M. & Brouzes, E. dPCR: A technology review. *Sensors* **18**, 1271 (2018).
17. Willmot, G. E. & Lin, X. S. *Mixed Poisson distributions* (Springer, New York, 2001).
18. Yang, J. & Hlavacek, W. S. Scaffold-mediated nucleation of protein signaling complexes: Elementary principles. *Mathematical Biosciences* **232**, 164–173 (2011).
19. Liao, P. et al. Three-dimensional digital PCR through light-sheet imaging of optically cleared emulsion. *Proceedings of the National Academy of Sciences* **117**, 25628–25633 (2020).
20. Serra, V. *et al.* PI3k inhibition results in enhanced HER signaling and acquired ERK dependency in HER2-overexpressing breast cancer. *Oncogene* **30**, 2547–2557 (2011-06).
21. Rockberg, J., Schwenk, J. M. & Uhlén, M. Discovery of epitopes for targeting the human epidermal growth factor receptor 2 (*HER2*) with antibodies. *Molecular Oncology* **3**, 238–247 (2009-06).
22. Vashist, S.K. & Luong, J.H. in *Chapter 4 - bioanalytical requirements and regulatory guidelines for immunoassays* (eds Vashist, S. K. & Luong, J. H.) *Handbook of Immunoassay Technologies* 81–95 (Academic Press, 2018).
23. Vashist, S.K. & Luong, J.H. in *Chapter 1 - immunoassays: An overview* (eds Vashist, S. K. & Luong, J. H.) *Handbook of Immunoassay Technologies* 1–18 (Academic Press, 2018).
24. Vashist, S.K. & Luong, J.H. in *Chapter 17 - immunoassays: Future prospects and possibilities* (eds Vashist, S. K. & Luong, J. H.) *Handbook of Immunoassay Technologies* 455–466 (Academic Press, 2018).
25. Feng, W. et al. Nulisa: a proteomic liquid biopsy platform with attomolar sensitivity and high multiplexing. *Nature Communications* **14**, 7238 (2023).
26. Assarsson, E. et al. Homogenous 96-plex pea immunoassay exhibiting high sensitivity, specificity, and excellent scalability. *PLoS ONE* **9**, e95192 (2014).
27. Lu, Y. *et al.* Highly multiplexed profiling of single-cell effector functions reveals deep functional heterogeneity in response to pathogenic ligands. *Proceedings of the National Academy of Sciences* **112** (2015).
28. Kraemer, S. *et al.* From somamer-based biomarker discovery to diagnostic and clinical applications: A somamer-based, streamlined multiplex proteomic assay. *PLoS ONE* **6**, e26332 (2011-10-17).
29. Ishikawa, K. Multilayered regulation of proteome stoichiometry. *Current Genetics* **67**, 883–890 (2021).
30. Bludau, I. & Aebersold, R. Proteomic and interactomic insights into the molecular basis of cell functional diversity. *Nature Reviews Molecular Cell Biology* **21**, 327–340 (2020-06).
31. Burke, D.F. *et al.* Towards a structurally resolved human protein interaction network. *Nature Structural & Molecular Biology* **30**, 216–225 (2023-02).
32. Llibre, A. et al. Development of an ultrasensitive digital immunoassay on the single molecule array (simoa) platform. *JoVE* **136**, 57421 (2018).
33. Genshaft, A. S. et al. Multiplexed, targeted profiling of single-cell proteomes and transcriptomes in a single reaction. *Genome Biology* **17**, 188 (2016).
34. Wenzl, T., Haedrich, J., Schaechtele, A., Robouch, P. & Stroka, J. *Guidance Document on the Estimation of LOD and LOQ for Measurements in the Field of Contaminants in Feed and Food* (Publications Office of the European Union, 2016).
35. Onsum, M. D. et al. Single-cell quantitative HER2 measurement identifies heterogeneity and distinct subgroups within traditionally defined HER2-positive patients. *The American Journal of Pathology* **183**, 1446–1460 (2013).
36. Emlet, D. R. et al. Response to trastuzumab, erlotinib, and bevacizumab, alone and in combination, is correlated with the level of human epidermal growth factor receptor-2 expression in human breast cancer cell lines. *Molecular Cancer Therapeutics* **6**, 2664–2674 (2007).
37. Concerns and recommendations in clinic and research. Mizrahi, O., Ish Shalom, E., Baniyash, M. & Klieger, Y. Quantitative flow cytometry. *Cytometry Part B: Clinical Cytometry* **94**, 211–218 (2018).

Acknowledgements

The authors thank Attila Karsai, Maike Smits, Bettina Moeckel, Georg Lentzen, Hardin Bolte, Martin Schwemmle, Zsolt Ruzsics and the Actome's team for constructive discussions. This work was supported in part by contracts of Ministerium für Wirtschaft, Arbeit und Wohnungsbau Baden-Württemberg PRIMO (Az: 3-4332.62-HSG/84) and DINAMIK (Az: 7533-7-11-10-06) and Baden-Württemberg Stiftung, MONOGRAM - MET-ID55. This work received financial support from the State Ministry of Baden-Wuerttemberg for Economic Affairs, Labour and Tourism.

Author contributions

C.J. conceived the presented method, provided overall direction and planning, and contributed to funding acquisition . T.G. assisted in coordinating the research, contributed to experimental and theoretical validation of the "equilibrium ternary binding" model, and finalized the figures. T.H. experimentally and theoretically validated the “compartment decouplexing” model. V.S. independently provided proof of the mathematical concept of the “compartment decouplexing” model. A.S. conducted mathematical analysis of the "equilibrium ternary binding" model. T.H. developed the code for evaluation. N.G. conducted antibody conjugation, experimental validation, and additional experiments on cellular materials for PICO validation. A.H. conducted SIMOA experiments, supervised by J.G. who also provided funding. P.K. offered scientific consulting and assistance with funding acquisition. M.B. produced recombinant Thioredoxin, performed quality control, and contributed to the quality control of recombinant ErbB2. N.K. and T.G. conducted PICO experiments on recombinant Thioredoxin and ErbB2. U.v.G. was the scientific supervisor at QIAGEN. P.P. provided laboratory facilities at QIAGEN, and R. Z. provided funding and laboratory facilities at the University of Freiburg. C.J. wrote the main manuscript text. All authors critically reviewed the manuscript.

Declarations

Competing interests

C.J. and P.K. have filed patents based on this work. C.J., P.K. and R.Z. are co-founders of Actome GmbH, N.G. and T.G. hold virtual shares in Actome GmbH. Qiagen is a shareholder of Actome. The remaining authors declare no competing financial interests.

Additional information

Supplementary Information The online version contains supplementary material available at https://doi.org/10.1038/s41598-025-91053-5.

Correspondence and requests for materials should be addressed to C.J.

Reprints and permissions information is available at www.nature.com/reprints.

Publisher’s note Springer Nature remains neutral with regard to jurisdictional claims in published maps and institutional affiliations.